energies

MDPI

Article

Development of Correlations Based on CFD Study for Microchannel Condensation Flow of Environmentally Friendly Hydrocarbon Refrigerants

Anıl Başaran [1] and Ali Cemal Benim [2,*]

1 Department of Mechanical Engineering, Engineering Faculty, Manisa Celal Bayar University, Manisa 45140, Turkey; anil.basaran@cbu.edu.tr
2 Center of Flow Simulation (CFS), Department of Mechanical and Process Engineering, Düsseldorf University of Applied Sciences, 40476 Düsseldorf, Germany
* Correspondence: alicemal@prof-benim.com; Tel.: +49-(0)-211-43-51-3504

Abstract: A CFD simulation of the condensation flow of R600a and R290 within microchannels was conducted to explore the effect of mass flux, hydraulic diameter, and vapour quality on heat transfer rate and pressure drop. Data obtained from CFD simulations were used to develop new heat transfer and pressure drop correlations for the condensation flows of R600a and R290, which are climate-friendly refrigerants. Steady-state numerical simulations of condensation flow of refrigerants were carried out inside a single circular microchannel with diameters varying between 0.2 and 0.6 mm. The volume of fluid approach was used in the proposed model, calculating the interface phase change using the Lee model. The CFD simulation model was validated via a comparison of the simulation results with the experimental data available in the literature. It is found that the newly developed Nu number correlation shows a deviation, with an Ave-MAE of 11.16%, compared to those obtained by CFD simulation. Similarly, the deviation between friction factors obtained by the newly proposed correlation and those obtained by CFD simulation is 20.81% Ave-MAE. Widely recognized correlations that are applicable to the condensation of refrigerants within small-scale channels were also evaluated by comparing newly developed correlations. It is concluded that the newly proposed correlation has a higher accuracy in predicting the heat transfer coefficient and pressure drop. This situation can contribute to the creation of a sustainable system via the use of microchannels and climate-friendly refrigerants, like R600a and R290.

Keywords: condensation flow; heat transfer coefficient; pressure drop; microchannel; CFD simulation; climate-friendly refrigerants; hydrocarbon refrigerants

check for updates

Citation: Başaran, A.; Benim, A.C. Development of Correlations Based on CFD Study for Microchannel Condensation Flow of Environmentally Friendly Hydrocarbon Refrigerants. *Energies* **2024**, *17*, 1531. https://doi.org/10.3390/en17071531

Academic Editors: Monika Rerak, Tomasz Sobota and Jan Taler

Received: 9 February 2024
Revised: 18 March 2024
Accepted: 19 March 2024
Published: 22 March 2024

1. Introduction

In heating, ventilating air conditioning, refrigeration systems (HVAC-R), and fluorinated greenhouse gases, especially Hydro-Fluoro-Carbons (HFCs), are widely used [1]. On the other hand, the significant contribution effect of these gases to global warming (GW) is a fact, recognized by both the United Nations Framework Convention on Climatic Change and the Kyoto Protocol [2]. As a response, in 2006, the European Union (EU) implemented a corresponding regulation, aiming to regulate their emissions and assigning corresponding global warming potential (GWP) values [3]. This regulation compelled numerous manufacturers in the sector to develop more efficient systems, capable of handling reduced refrigerant volumes and utilizing alternative low-GWP refrigerants, such as hydrocarbons (HCs). Hydrocarbon (HCs) refrigerants, such as refrigerants R600a (isobutane) and R290 (propane), are environmentally friendly compounds that present a viable option to replace refrigerants with potential environmental hazards [4–6]. Specifically, R600a (isobutane) and R290 (propane) refrigerants stand out as favorable substitutes, owing to their notable advantages, such as zero ozone depletion potential, minimal contribution to GWP, minimal toxicity, and low costs [5,6]. Moreover, refrigerants R290 and R600a align with the requirements of the EU F-gas regulations, further enhancing their appeal.

Overcoming the challenge of achieving high heat transfer rates within small spaces has long been a central concern in the realm of heat exchanger design. Thanks to recent advancements in micro-manufacturing techniques, microchannel heat exchangers (MCHEs) have become an emerging alternative to conventional heat exchangers to overcome compactness problems. Prominent advantages associated with the MCHEs include their compact design and enhanced overall heat transfer coefficient [7,8]. In other words, MCHEs present a promising solution due to their inherent advantages. Due to their noticeable advantages, MCHEs have gained significant popularity in various industrial applications, such as heating, ventilating, air-conditioning and refrigeration (HVAC-R), electronic cooling, and heat pumps and medical devices [4,5]. In these applications, the system is typically designed to facilitate a phase change of the working fluid, usually a refrigerant, in the condenser/evaporator. However, it is important to note that microchannels introduce different flow regimes and heat transfer mechanisms compared to conventional channels as the hydraulic diameter decreases [9,10]. Essentially, the significance of surface tension relative to gravitational forces amplifies with a reduction in the hydraulic diameter [4,11]. Consequently, understanding the fluid flow and heat transfer characteristics of microchannel condensation is crucial for optimizing condenser performance. The use of heat transfer and pressure drop correlations is a very common and practical approach to understanding the fluid flow and heat transfer characteristics in condenser modeling. The correlations developed for the condensation flow of refrigerants inside small-scale channels are shown in Tables 1 and 2. Table 1 indicates heat transfer coefficient correlations while Table 2 shows pressure drop correlations. According to Tables 1 and 2, experimental studies on the condensation flows of R600a and R290 in the microchannel are quite limited in the literature. It is considered that the main reason for this situation is the explosive and flammable features of R600a and R290. These features of R600a and R290, like other hydrocarbons, can create a safety risk for experimental studies.

Table 1. Widely recognized correlations for the heat transfer coefficient for the condensation of refrigerants within small-scale channels [4].

Researcher	Correlations	Range and Applicability
Dobson and Chato [12]	$\mathrm{Nu} = 0.023\mathrm{Re}_l^{0.8}\mathrm{Pr}_l^{0.4}\left(1 + \frac{2.22}{X_{tt}^{0.89}}\right)$ $\mathrm{Fr}_{So} = \begin{cases} 0.025\mathrm{Re}_l^{1.59}\left(\frac{1+1.09X_{tt}^{0.039}}{X_{tt}}\right)\frac{1}{\mathrm{Ga}^{0.5}}, & \mathrm{Re}_l \leq 1250 \\ 1.26\mathrm{Re}_l^{1.04}\left(\frac{1+1.09X_{tt}^{0.039}}{X_{tt}}\right)\frac{1}{\mathrm{Ga}^{0.5}}, & \mathrm{Re}_l > 1250 \end{cases}$	D_h = 4.6, 7.04, and 31.4 mm Near-azeotropic blends of R32/R125 R134a, R12, R22, G = 25–800 kg/m^{2}s T_{sat} = 35–60 °C
Moser et al., 1998 [13]	$\mathrm{Nu} = \frac{0.0994^{0.126\times\mathrm{Pr}_l^{-0.448}}\mathrm{Re}_l^{-0.113\times\mathrm{Pr}_l^{-0.563}}\mathrm{Re}_{eq}^{1+0.11025\times\mathrm{Pr}_l^{-0.448}}\mathrm{Pr}_l^{0.815}}{\left[1.58\times\ln(\mathrm{Re}_{eq})-3.28\right]\left[2.58\times\ln(\mathrm{Re}_{eq})+13.7\mathrm{Pr}_l^{2/3}-19.1\right]}$ $\mathrm{Re}_{eq} = \varnothing_{lo}^{8/7}\mathrm{Re}_{lo},\ \varnothing_{lo}^2 = A_1 + \frac{3.24A_2}{\mathrm{Fr}_{TP}^{0.045}\mathrm{We}_{TP}^{0.035}}$ $A_1 = (1-x)^2 + x^2\left(\frac{\rho_l}{\rho_v}\right)\left(\frac{f_{vo}}{f_{lo}}\right),$ $A_2 = x^{0.78}(1-x)^{0.24}\left(\frac{\rho_l}{\rho_v}\right)^{0.91}\left(\frac{\mu_v}{\mu_l}\right)^{0.19}\left(1-\frac{\mu_v}{\mu_l}\right)^{0.7}$	R22, R134a, R410A, R12, R125, R11 D_h = 3.14–20 mm

Table 1. *Cont.*

Researcher	Correlations	Range and Applicability
Koyama et al., 2003 [14]	$\mathrm{Nu} = \left(\mathrm{Nu}_F^2 + \mathrm{Nu}_B^2\right)^{1/2}$ $\mathrm{Nu}_F = 0.0152\left(1 + 0.6\mathrm{Pr}_l^{0.8}\right)\left(\frac{\varnothing_v}{X_{tt}}\right)\mathrm{Re}_l^{0.77}$ $\varnothing_v^2 = 1 + 21\left(1 - e^{-0.319D_h}\right)X_{tt} + X_{tt}^2$ $\mathrm{Nu}_B = 0.725H(\xi)\left(\frac{GaPr_l}{Ph}\right)^{1/4}$ $\xi = \left[1 + \frac{\rho_v}{\rho_l}\left(\frac{1-x}{x}\right)\left(0.4 + 0.6\sqrt{\frac{\frac{\rho_l}{\rho_v} + 0.4\frac{1-x}{x}}{1 + 0.4\frac{1-x}{x}}}\right)\right]^{-1}$	R134a Multiport rectangular D_h = 0.8 and 1.11 mm G = 100–700 kg/m^2s T_{sat} = 60 °C
Cavallini et al., 2006 [15]	**ΔT⁻independent flow regime ($J_G > J_G^T$):** $\mathrm{HTC}_A = \mathrm{HTC}_{lo}\left[1 + 1.128x^{0.817}\left(\frac{\rho_l}{\rho_v}\right)^{0.3685}\left(\frac{\mu_v}{\mu_l}\right)^{0.2363}\left(1 - \frac{\mu_v}{\mu_l}\right)^{2.144}\mathrm{Pr}_l^{-0.1}\right]$ $\mathrm{HTC}_{lo} = 0.023\mathrm{Re}_{lo}^{0.8}\mathrm{Pr}_l^{0.4}\frac{k_l}{D_h}$ **ΔT⁻depended flow regime ($J_G < J_G^T$):** $\mathrm{HTC}_D = \left[\mathrm{HTC}_A\left(\frac{J_G^T}{J_G}\right)^{0.8} - \mathrm{HTC}_{STRAT}\right]\frac{J_G}{J_G^T} + \mathrm{HTC}_{STRAT}$ $\mathrm{HTC}_{STRAT} =$ $0.725\left\{1 + 0.741\left(\frac{1-x}{x}\right)^{0.3321}\right\}^{-1} \times \left[\frac{k_l^3\rho_l(\rho_l - \rho_v)g\Delta h_{vl}}{\mu_l D_h \Delta T}\right]^{0.25} + \left(1 - x^{0.087}\right)h_{lo}$	R134a, R236ea, R410A D_h = 0.4–3 mm
Son and Lee, 2009 [16]	$\mathrm{Nu} = 0.034\mathrm{Re}_l^{0.8}\mathrm{Pr}_l^{0.3}f_c(X_{tt})$ $f_c(X_{tt}) = \left[3.28\left(\frac{1}{X_{tt}}\right)^{0.78}\right]$	R22, R134a, and R410A Single smooth D_h = 1.77, 3.36 and 5.35 mm G = 200–400 kg/m^2s T_{sat} = 40 °C
Huang et al., 2010 [17]	$\mathrm{Nu} = 0.0152\left(-0.33 + 0.83\mathrm{Pr}_l^{0.8}\right)\frac{\varnothing_v}{X_{tt}}\mathrm{Re}_l^{0.77}$ $\varnothing_v = 1 + 0.5\left[\frac{G}{\sqrt{g\rho_v(\rho_l - \rho_v)D_h}}\right]X_{tt}^{0.35}$	R410A and R410A-oil D_h = 1.6 and 4.18 mm G = 200–600 kg/m^2s T_{sat} = 40 °C X_{inlet} = 0.3–0.9
Park et al., 2011 [18]	$\mathrm{Nu} = 0.0055\mathrm{Pr}_l^{1.37}\frac{\varnothing_v}{X_{tt}}\mathrm{Re}_l^{0.7}$ $\varnothing_v = 1 + 13.17\left(\frac{\rho_v}{\rho_l}\right)^{0.17}\left[1 - \exp\left(-0.6\sqrt{\frac{g(\rho_l - \rho_v)D_h^2}{\sigma}}\right)\right]X_{tt} + X_{tt}^2$	R134a, R236fa, R1234ze Multichannel, rectangular, vertical D_h = 1.45 mm G = 50–260 kg/m^2s T_{sat} = 25–70 °C
Bohdal et al., 2011 [19]	$\mathrm{Nu} = 25.084\mathrm{Re}_l^{0.258}\mathrm{Pr}_{lp}^{-0.495}p_r^{-0.288}\left(\frac{x}{1-x}\right)^{0.266}$ $p_r = \frac{p_{sat}}{p_{cr}}$	R134a and R404A Circular D_h = 0.31–3.30 mm G = 100–1300 kg/m^2s T_{sat} = 20–40 °C
Shah, 2016 [20]	**Correlation #1** $\mathrm{HTC}_I = \mathrm{HTC}_{lo}\left[\left(1 + \frac{3.8}{Z^{0.95}}\right)\left(\frac{\mu_l}{14\mu_v}\right)^{(0.0058 + 0557P_r)}\right]$ $\mathrm{HTC}_{Nu} = 1.32\mathrm{Re}_{lo}^{-1/3}\left[\frac{k_l^3\rho_l(\rho_l - \rho_v)g}{\mu_l^2}\right]^{1/3}$ $\mathrm{HTC}_{lo} = 0.023\mathrm{Re}_{lo}^{0.8}\mathrm{Pr}_l^{0.4}\frac{k_l}{D_h}$ **Correlation #2** $\mathrm{HTC}_{II} = \mathrm{HTC}_{lo}\left[1 + 1.128x^{0.817}\left(\frac{\rho_l}{\rho_v}\right)^{0.3685}\left(\frac{\mu_v}{\mu_l}\right)^{0.2363}\left(1 - \frac{\mu_v}{\mu_l}\right)^{2.144}\mathrm{Pr}_l^{-0.1}\right]$	33 types of refrigerant, all geometrical combinations D_h = 0.10–49.0 mm G = 1.1–1400 kg/m^2s

Table 2. Widely recognized correlations for the pressure drop during the condensation of refrigerants within small-scale channels [4].

Researcher	Correlations	Range and Applicability
Lockhart and Martinelli, 1949 [21]	$\frac{\Delta P}{L} = \varnothing_l^2 \left(\frac{dP}{dz}\right)_l$ $\varnothing_l^2 = 1 + \frac{C}{X} + \frac{1}{X^2},\quad X = \left[\frac{\left(\frac{dP}{dz}\right)_v}{\left(\frac{dP}{dz}\right)_l}\right]^{1/2}$ $C = \begin{cases} 20, & \text{Liquid : Turbulent/Vapor : Turbulent} \\ 12, & \text{Liquid : Laminar/Vapor : Turbulent} \\ 10, & \text{Liquid : Turbulent/Vapor : Laminar} \\ 5, & \text{Liquid : Laminar/Vapor : Laminar} \end{cases}$	Benzene, kerosene, water and various oils D_h = 1.488–25.83 mm
Friedel, 1979 [22]	$\frac{\Delta P}{L} = \varnothing_{lo}^2 \left(\frac{dP}{dz}\right)_{lo}$ $\varnothing_{lo}^2 = E + \frac{0.32FH}{Fr_{TP}^{0.045} We_{TP}^{0.035}}$ $E = (1-x)^2 + x^2 \frac{\rho_l f_{vo}}{\rho_v f_{lo}},\qquad F = x^{0.78}(1-x)^{0.24}$ $H = \left(\frac{\rho_l}{\rho_v}\right)^{0.91}\left(\frac{\mu_v}{\mu_l}\right)^{0.19}\left(1 - \frac{\mu_v}{\mu_l}\right)^{0.7}$	Adiabatic $D_h > 1$ mm
Mishima and Hibiki, 1996 [23]	$\frac{\Delta P}{L} = \varnothing_l^2 \left(\frac{dP}{dz}\right)_l$ $\varnothing_l^2 = 1 + \frac{C}{X} + \frac{1}{X^2},\qquad C = 21\left(1 - e^{-0.319D}\right)$	Water–air mixture Single circular–vertical D_h = 1–4 mm
Garimella et al., 2005 [24]	$\frac{\Delta P}{L} = \frac{1}{2} f_i \rho_v \frac{G^2 x^2}{\rho_v \propto^{2.5}} \frac{1}{D_h}$ $\frac{f_i}{f_l} = A X^a {Re_{l,\propto}}^b \varphi^c$ $\text{If } Re_{l,\propto} < 2100 \begin{cases} A = 1.308 \times 10^{-3} \\ a = 0.4273 \\ b = 0.9295 \\ c = -0.1211 \end{cases}$ $\text{If } Re_{l,\propto} > 3400 \begin{cases} A = 25.64 \\ a = 0.532 \\ b = -0.327 \\ c = 0.021 \end{cases}$ $\varphi = \frac{J_l \mu_l}{\sigma},\qquad J_l = \frac{G(1-x)}{\rho_l(1-\propto)}$	R134a Circular D_h = 0.5–4.91 mm G = 150–750 kg/m^2s
Cavallini et al., 2002 [25]	$\frac{\Delta P}{L} = \varnothing_{lo}^2 \left(\frac{dP}{dz}\right)_{lo}$ $\varnothing_{lo}^2 = E + \frac{1.262FH}{We^{0.1458}}$ $E = (1-x)^2 + x^2 \frac{\rho_l f_{vo}}{\rho_v f_{lo}},\qquad F = x^{0.6978}$ $H = \left(\frac{\rho_l}{\rho_v}\right)^{0.3278}\left(\frac{\mu_v}{\mu_l}\right)^{-1.181}\left(1 - \frac{\mu_v}{\mu_l}\right)^{3.477}$	R-22, R-134a, R-125, R-32, R-236ea, R-407C, and R-410A Circular D_h = 8 mm G = 100–750 kg/m^2s T_{sat} = 30–50 °C
Bohdal et al., 2011 [19]	$\left(\frac{dP}{dz}\right)_f = \left(\frac{dP}{dz}\right)_{lo}\left[0.003\left(\frac{P_{sat}}{P_{cr}}\right)^{-4.722} E^{-0.992} + 143.74\left(\frac{F^{0.671}H^{-0.019}}{We^{0.308}}\right)\right]$ $E = (1-x)^2 + x^2 \frac{\rho_l f_{vo}}{\rho_v f_{lo}},\qquad F = x^{0.98}(1-x)^{0.24}$ $H = \left(\frac{\rho_l}{\rho_v}\right)^{0.91}\left(\frac{\mu_v}{\mu_l}\right)^{0.19}\left(1 - \frac{\mu_v}{\mu_l}\right)^{0.7}$ $f_x = 8\left[\left(\frac{8}{Re_x}\right) + \left\{2.457 \times \ln\left[\left(\frac{Re_x}{7}\right)^{0.9}\right]^{16} + \left(\frac{37530}{Re_x}\right)^{16}\right\}^{-1.5}\right]^{1/12}$	R134a, R404A, R407C Single circular D_h = 0.31–3.3 mm G = 0–1300 kg/m^2s T_{sat} = 20–50 °C
Son and Oh, 2012 [26]	$\frac{\Delta P}{L} = \varnothing_l^2 \left(\frac{dP}{dz}\right)_l$ $\varnothing_l^2 = 1 + \frac{C}{X} + \frac{1}{X^2},$ $C = 2485 We_{TP}^{0.407} Re_{TP}^{0.34}$	R22, R134a, and R410A Single circular D_h = 1.77 mm G = 450–1050 kg/m^2s T_{sat} = 40 °C
Sakamatapan and Wongwises, 2014 [27]	$\frac{\Delta P}{L} = \frac{2 \times f_{TP} \times Re_{eq}^2 \times \mu_l^2}{\rho_l {D_h}^3}$ $f_{TP} = 6977 Re_{eq}^{-0.337} x^{-0.031}\left(\frac{\rho_l}{\rho_v}\right)^{6.510}\left(\frac{\mu_v}{\mu_l}\right)^{-11.883}$ $Re_{eq} = \frac{G_{eq} D_h}{\mu_l},\qquad G_{eq} = G\left[(1-x)x\sqrt{\frac{\rho_l}{\rho_v}}\right]$	R134a, Multiport D_h = 1.1 and 1.2 mm G = 345–658 kg/m^2s T_{sat} = 35–45 °C

Table 2. *Cont.*

Researcher	Correlations	Range and Applicability
Lopez-Belchi et al., 2014 [28]	$\left(\frac{dP}{dz}\right)_{TP} = \varnothing_l^2 \left(\frac{dP}{dz}\right)_l$ $\varnothing_l^2 = 1 + \frac{C}{X} + \frac{1}{X^2}$, $X^2 = \frac{(dP/dz)_l}{(dP/dz)_v}$ $\left(\frac{dP}{dz}\right)_l = \frac{2f_l G^2 (1-x)^2}{D_h \rho_l}$, $\left(\frac{dP}{dz}\right)_v = \frac{2f_v G^2 x^2}{D_h \rho_v}$ $f_x = \begin{cases} \frac{16}{Re_x}, & Re_x < 2000 \\ 0.25(1.1525Re_x + 895) \times 10^{-5}, & 2000 \le Re_x < 3000 \\ \frac{1}{16}\left[\log\left(\frac{150.39}{Re_x^{0.98865}} - \frac{152.66}{Re_x}\right)\right]^{-2}, & Re_x \ge 3000 \end{cases}$	R1234yf, R134a, and R32 Round D_h = 1.16 mm G = 350–940 kg/m^{2}s T_{sat} = 20–55 °C

Utilizing numerical simulations proves to be a valuable approach for comprehending microchannel condensation in the absence of dedicated experimental data or correlations. To minimize both the cost and effort associated with experimentation, the development of numerical models independent of specific geometry and fluid properties has gained increasing significance [4,11]. In this context, numerical methods, especially those based on the volume of fluid (VOF) method, have begun to be used in recent years for industrial microfluidic devices such as micro-reactors [29] and aviation microfluidic equipment [30]. Similarly, numerous numerical studies can be found in the literature, which were conducted to explore the heat transfer and pressure drop characteristics of the condensation flow of refrigerants inside microchannels. Numerical simulations were conducted by Chen et al. [31] to model the condensation flow of refrigerant FC-72 within a rectangular microchannel with a hydraulic diameter of 1 mm. They used the VOF method to predict condensing flow in their model. Turbulence was accounted for using the realizable k-ε model. Their simulations revealed that a reduction in wall cooling heat flux or an increase in flow mass flux resulted in an elongation of the vapour column. Ganapathy et al. [32] presented a numerical simulation model based on the VOF method to simulate the fluid flow and heat transfer characteristics that are present during condensation in a single microchannel. They conducted a two-dimensional transient simulation for the condensation of R134a within a microchannel (D = 100 μm). In their simulations, the inlet vapour mass flux varied between 245 and 615 kg/m^{2}s, while the heat flux ranged from 200 to 800 kW/m^2. Bortolin et al. [33] conducted numerical simulations in a steady state to investigate the condensation of R134a within a 1 mm square minichannel. The simulations utilized the VOF method to track the vapour–liquid interface throughout the condensation flow. Mass fluxes with values between 400 and 800 kg/m^{2}s were considered, while maintaining a uniform wall temperature as the boundary condition. The numerical model treated both the vapour core and liquid film as turbulent phases, employing a low-Reynolds-number version of the Shear Stress Transport (SST) k-ω model. The authors concluded that, in the square minichannel, gravity had a negligible impact, and the heat transfer mechanism was primarily influenced by shear stress and surface tension at the considered mass fluxes. Zhang et al. [34] performed a numerical investigation of the heat transfer and pressure drop characteristics during the condensation of R410A within horizontal microchannel tubes with hydraulic diameters of 0.25, 1, and 2 mm. They took into consideration the effect of various saturation temperatures on heat transfer and fluid flow. Their primary emphasis was on assessing the impact of the saturation temperature (T_{sat}) of R410 refrigerant on the heat transfer and pressure drop characteristics. The study employed the VOF model and, for both vapour and liquid phases, the SST-k-ω turbulent model was utilized. Tonelli et al. [35] carried out steady-state numerical simulations to examine R134a condensation within horizontal channels, analyzing the impact of diameters (1 and 3.4 mm) on heat transfer and two-phase flow. Additionally, they conducted two-dimensional transient simulations to analyze the influence of waves on the condensation flow. The simulations employed the VOF method at T_{sat} = 40 °C and mass fluxes ranging from 50 to 200 kg/m^{2}s. According to their steady-state numerical simulations, it was observed that reducing the channel diameter from 3.4 to 1 mm led to an increase in the heat transfer coefficient, and the effect of surface tension on the liquid film distribution was found to be negligible in the 3.4 mm channel. Wu and Li [36] introduced a transient numerical simulation model to analyze the heat transfer and fluid flow characteristics during condensation. Their study was concentrated on simulating the condensation flow of R32 within a circular tube with a diameter of 0.1 mm. The authors could model four distinct flow patterns (annular, injection flow, slug flow, and bubbly flow) within a two-dimensional computational domain. Da Riva and Del Col [37] carried out simulations on the condensation of R134a within a 1 mm inner diameter minichannel with a circular cross-section, considering both high (G = 800 kg/m^{2}s) and low (G = 100 kg/m^{2}s) mass fluxes. Their study encompassed the effects of interfacial shear stress, gravity, and surface tension, with a particular focus on horizontal tube orientation. The subsequent steps involved simulating the same conditions for vertical downflow with normal gravity, as well as simulations without gravity effects. In related work, Da Riva and Del Col [38] presented a numerical simulation model for laminar liquid film condensation in a horizontal circular minichannel with an internal diameter of 1 mm. Utilizing the VOF method, a three-dimensional simulation was conducted of the laminar fluid film condensation of R134a inside the minichannel. The simulations were executed with and without considering surface tension to examine its effect under the specified conditions.

It is worth noting that the current body of literature does not provide a comprehensive predictive tool that can handle a wide range of working fluids, mass flow rates, pressures, channel geometries, and channel sizes [4,11]. Previous experimental and numerical investigations primarily focused on the condensation flow of hydrofluorocarbon (HFC) refrigerants, like R134a, and refrigerant blends within microchannels. On the other hand, R290 and R600a are climate-friendly refrigerant substitutes, which are aligned with the requirements of the EU F-gas regulation. Thus, similar to microchannel heat exchangers, they are also important in HVAC-R applications. A predictive tool for fluid flow that applies to the condensation flow of R600a and R290 inside microchannels is still lacking in the literature. In this respect, the goal of the current study is to develop heat transfer coefficient and pressure drop correlations with high predictivity within a microchannel during the condensation of R600a and R290. To achieve this, correlations were developed based on numerical simulations of R600a and R290 condensation. The steady-state calculations were carried out within a single circular microchannel with varying diameters below 1 mm (0.2, 0.4, and 0.6 mm) and at mass fluxes between 200 and 600 kg/m^{2}s. The numerical modeling approach presented in this current study was verified using experimental data for R134a condensation inside a circular microchannel available in the literature. This validated simulation model was applied to predict the R600a and R290 condensation heat transfer coefficient and friction factor for pressure drops. The obtained numerical results were used to derive new heat transfer coefficient and friction factor correlations. New correlations for heat transfer coefficient and pressure drop were developed for R600a and R290 condensation inside microchannels based on the numerical simulation results. Thus, the gap in the literature was filled and the highly predictive model's needs during heat design calculations were met. In this regard, the study contributes to the design of high-performance microchannel condensers for climate-friendly refrigerants that are widely used in HVAC-R devices.

2. Materials and Methods

2.1. Numerical Simulation Conditions

In this study, numerical simulations were performed to investigate the condensation of refrigerants R600a and R290 within smooth, circular microchannels with various diameters (0.2, 0.4, and 0.6 mm), assuming a steady-state flow. The simulations covered mass fluxes between 200 and 600 kg/m^{2}s, considering different inlet thermodynamic vapour qualities between 0.3 and 0.9. For the velocity components, the no-slip condition applies at the wall. The thermal boundary condition at the wall was a prescribed heat flux of 40 kW/m^2. The condensation simulations for R600a and R290 refrigerants were carried out while assuming T_{sat} to be 40 °C. The thermophysical properties of R600a and R290 corresponding to this saturation temperature are indicated in Table 3.

Table 3. Thermophysical properties of refrigerants R600a and R290 (T_{sat} = 40 °C [39]).

	R600a		**R290**	
	Vapour	**Liquid**	**Vapour**	**Liquid**
Density (kg/m^3)	13.7	531.2	30.165	467.46
Viscosity (Pa-s)	0.00000791	0.000129	0.0000088918	0.000082844
Specific heat (kJ/kg-K)	1.921	2.5349	2.2632	2.9127
Thermal conduct. (W/m-K)	0.018524	0.084051	0.021432	0.0866923
Prandtl number (-)	0.82056	3.9024	0.93896	2.776
Saturation pressure (kPa)	531.21		1369.4	
Surface tension (N/m)	0.0084105		0.0052128	

2.1.1. Assumptions for Numerical Simulations

An axisymmetric, steady-state flow assumption is made, with the neglect of gravity and potential flow instabilities. It is apparent that steady-state simulations cannot capture flow instabilities, including interfacial waves. Therefore, the justification for the chosen modeling approach needs to be established. One method of justification lies in consulting flow pattern maps available in the literature. A widely acknowledged flow pattern map is the one introduced by Coleman and Garimella [40]. According to Coleman and Garimella's map [40], it is expected that the flow regime will be annular flow for the conditions considered in the current simulations.

Under the simulation conditions in question, the occurring pressure variations were relatively low compared to the condensation pressure (531.21 kPa for R600a and 1369.4 kPa for R290). Consequently, pressure variations in the channels were neglected, and the T_{sat} was considered to be constant for both refrigerants. This assumption was made on the premise that there would be no alteration in the thermophysical properties of refrigerants R600a and R290. As mentioned previously, during microchannel condensation flow, surface tension can supersede the influence of gravity. To assess the relative effects of the gravity and surface tension, the criteria based on Bond number were considered. Two Bond number-based criteria discussed by Li and Wang [41] and Nema et al. [42] were employed. The Bond number (Bo) and the critical Bond number ($\mathrm{Bo_{cr}}$) can be expressed as follows:

$$\mathrm{Bo} = \frac{g(\rho_l - \rho_v)D_h^2}{\sigma} \tag{1}$$

$$\mathrm{Bo_{cr}} = \frac{1}{\left(\frac{\rho_l}{\rho_l - \rho_v} - \frac{\pi}{4}\right)} \tag{2}$$

Based on previous research by Li and Wang [41], the influence of gravity can be disregarded when the Bond number (as defined in Equation (1)) is below 0.05. Additionally, as suggested by Nema et al. [42], the effects of small tube diameters (related to forces due to surface tension) take precedence when the critical Bond number ($\mathrm{Bo_{cr}}$) surpasses the actual Bond number (Bo). Both these criteria, in our study, indicated that gravity played a minor role in the cases under consideration. As a result, gravitational forces were not considered in the current calculations. Note that, for both the liquid and vapour phases, an incompressible flow was assumed.

2.1.2. Computational Domain and Mesh Generation

In the proposed two-dimensional, axisymmetric formulation, the solution domain representing the microchannel is a rectangle. The tube's inner diameter changes from 0.2 to 0.6 mm. The domain length was assumed to be 5 mm. Figure 1 depicts the solution domain.

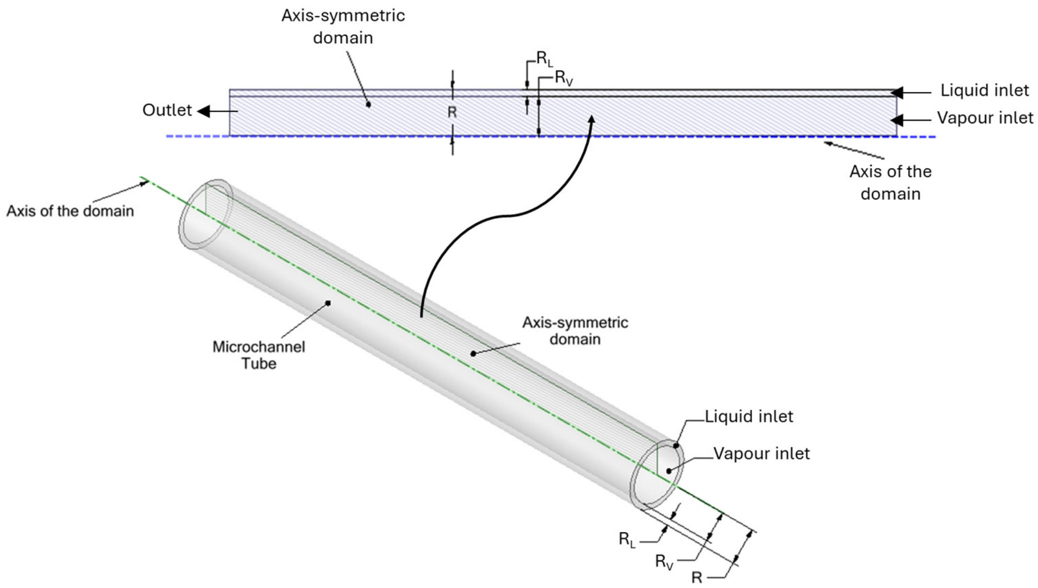

Figure 1. Solution domain with indication of boundaries.

During condensation flow, it is expected that the liquid will become a film on the microchannel wall while the vapour forms in the microchannel core. Therefore, two inlet boundaries for the liquid (R_l) and vapour (R_v) were separately specified at the microchannel inlet. The inlet velocities of the liquid (u_l) and vapour phases (u_v) were computed based on mass flux (G) and quality (x), as in Equations (3) and (4):

$$u_l = \frac{(1-x)GD^2}{\rho_l\left(D^2 - D_v^2\right)} \tag{3}$$

$$u_v = \frac{xGD^2}{\rho_l D_v^2} \tag{4}$$

Rectangular finite volumes were used for the discretization. The applied grid structure is displayed in Figure 2. To achieve a sufficiently fine resolution of the liquid layer, and to ensure y+ values lower than 1, a local grid refinement in the radial direction was applied near the wall. A grid independence study was performed based on five different grids, with cell counts between 12,750 and 156,000. For cell counts larger than 51,000, the variations observed for heat transfer coefficients and wall temperatures were smaller than 0.02% and 2.11%, respectively. Thus, the mesh with 51,000 cells was found to be sufficiently adequate and used in the analysis.

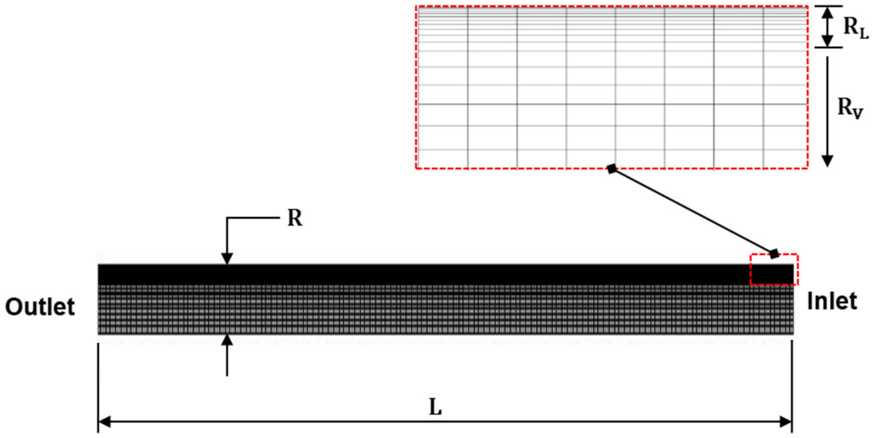

Figure 2. The mesh with detail views.

2.1.3. Governing Equations

The Volume of Fluid (VOF) method [43] was used to model the present condensing two-phase flow. The Volume of Fluid (VOF) method relies on defining a scalar volume fraction (α_i) to represent the proportion of the computational cell volume occupied by a specific phase (i). These values are then transported using the velocity field. Within the VOF model framework, the calculation of thermophysical properties for a two-phase mixture depends on the assignment of volume fractions to each cell, which is determined in the following manner:

$$\varphi_{eff} = \varphi_l \alpha_l + \varphi_v (1 - \alpha_l) \tag{5}$$

where φ_{eff} represents the effective thermophysical properties of the mixture (two-phase). In the VOF approach, the continuity equations for liquid and vapour can be written as follows:

$$\vec{u} \nabla \alpha_l = \frac{S_l}{\rho_l} \text{ and } \vec{u} \nabla \alpha_v = \frac{S_v}{\rho_v} \tag{6}$$

In the VOF model, the momentum equations describing the distinct phases interact through the interfacial forces, encompassing the contributions of surface tension. The modeling of these interfacial forces is computed by the Continuum Surface Force (CSF) methodology established by Brackbill et al. [44]. In this model, the interface curvature is also taken into account:

$$\nabla \cdot \left(\rho_{eff} \vec{u} \vec{u}\right) = -\nabla p + \nabla \cdot \left[\mu_{eff} \left(\nabla \vec{u} + \vec{u}^T\right)\right] + \rho_{eff} \vec{g} + \vec{F}_{vol} \tag{7}$$

$$\vec{F}_{vol} = \sigma \frac{\rho \kappa \nabla \alpha_l}{(\rho_l + \rho_v)} \tag{8}$$

$$\kappa = \nabla \frac{\nabla \alpha_l}{|\nabla \alpha_l|} \tag{9}$$

In the above equations, the variables κ and σ denote the interface curvature and surface tension, respectively. The volume force caused by the latter is denoted by $\vec{F}_{vol}$.

The energy equation is depicted below:

$$\nabla . \left(\vec{u} \rho h\right) = \nabla \cdot (\lambda_{eff} \nabla T) + S_E \tag{10}$$

where λ_{eff} stands for the effective thermal conductivity. The source term due to phase change is denoted by S_E, the calculation of which is shown below:

$$S_E = S_v h_{lv} = S_l h_{lv} \tag{11}$$

where h_{lv} represents the vaporization enthalpy for phase change. A weighted average approach is applied to compute the specific sensible enthalpy (h):

$$h = \frac{\alpha_l \rho_l h_l + \alpha_v \rho_v h_v}{\alpha_l \rho_l + \alpha_v \rho_v} \tag{12}$$

The phase change mass transfer was calculated using the model of Lee [14].

$$S_v = -S_l = \beta \alpha_v \rho_v \frac{T - T_{sat}}{T_{sat}}, \text{ for condensation} \quad (T < T_{sat}) \tag{13}$$

$$S_v = -S_l = \beta \alpha_l \rho_l \frac{T - T_{sat}}{T_{sat}}, \text{ for evaporation} \quad (T \geq T_{sat}) \tag{14}$$

where T denotes the local temperature, whereas T_{sat} represents the saturation temperature. In Equations (13) and (14), β is an adjustable positive constant. The selection of appropriate β values is a key challenge in the application of the Lee model due to the fact that there are many recommended optimum β values, which depend on many factors, such as mesh size, flow rate, and specific phase change factors, for similar problems. β values between 5×10^5 and 4×10^6 were used in the current study. In this range, the difference between T_{sat} and the predicted interface temperatures did not exceed 1 K.

2.1.4. Further Aspect of Numerical Approach

The condensation numerical simulations were conducted using the ANSYS Fluent 2023-R1 (Academic Version) [45], which is a general-purpose Computational Fluid Dynamics (CFD) code based on the finite volume method. As clarified earlier, the primary focus of this study was to model condensing two-phase flow in steady state, within the framework of a Reynolds Averaged Numerical Simulation (RANS) formulation [46]. While more advanced turbulence closure models are available [47,48], a turbulence viscosity-based model [49] was deemed sufficient for the current investigation. Specifically, the Shear Stress Transport (SST) k-ω model [50] was used to model turbulence. The Semi-Implicit Method for Pressure-Linked Equations (SIMPLE) scheme was used for pressure-velocity coupling. The third-order MUSCL scheme was applied to discretize the differential balance equations, encompassing momentum, energy, and turbulence equations. Pressure was treated via the PREssure STaggering Option (PRESTO) scheme, while the modified High-Resolution Interface-Capturing (HRIC) scheme was applied for the volume fraction.

2.1.5. Verification of the Computational Model

To validate the computational model proposed in this study, a comparison was conducted between the simulation results and the measurements available in the literature. In this context, the benchmark for the current investigation was established based on the measurements of Shin and Kim [51]. In other words, the heat transfer coefficients predicted by the proposed numerical simulation model were compared with the measured values presented by Shin and Kim [51]. For the comparison, a condensation simulation of R134a inside a horizontal microchannel with a diameter of 0.493 mm was performed. Table 4 illustrates the deviations between the simulated heat transfer coefficients and those derived from the experiments conducted by Shin and Kim [51]. Table 4 also indicate deviations between heat transfer coefficients calculated using existing correlations in the literature and the measurements of Shin and Kim [51]. According to Table 4, the difference between the simulation and experimental results shows a slight increase, with higher inlet vapour quality, but the maximum relative deviation remains under 26%. The average relative deviation between simulation prediction and experimental data of Shin and Kim [51] remains approximately 14.3%, which is below the relative deviation of other existing correlations, except the Shah correlation [20]. Based on the average mean absolute error (MAE), the Shah correlation [20], exhibiting an average MAE of 13.1%, performs slightly better than the present simulations. On the other hand, the performance of Shah correlation [20] does not remain stable with varying inlet quality. Furthermore, it should be emphasized that, in the experiments conducted by Shin and Kim [51], a reported uncertainty of ±12.9% was associated with the measured heat transfer rate. In this respect, it can be concluded that the MAE of 14.3% between the experimental data of Shin and Kim [51] and the current simulation is acceptable.

Table 4. The deviations of the simulated and correlated heat transfer coefficients from the heat transfer coefficients obtained by the experiments of Shin and Kim [51] in terms of MAE.

G (kg/m^2s)	Inlet x	MAE of Simulation	MAE of Condensation Correlations (%)								
			Dobson and Chato [12].	Moser et al. [13]	Koyama et al. [14]	Cavallini et al. [15]	Son and Lee [16]	Huang et al. [17]	Park et al. [18]	Bohdal et al. [19]	Shah [20]
200	0.305	**10.14**	16.8	22.1	68.9	34.0	17.4	37.1	78.4	193.8	2.5
	0.515	**20.82**	14.8	28.2	65.6	33.5	25.9	32.9	78.5	160.5	1.8
	0.734	**22.06**	19.9	36.1	62.3	37.5	16.4	36.8	78.7	120.0	10.6
	0.815	**24.80**	25.7	41.3	62.4	41.9	5.4	41.6	79.3	97.7	17.1
400	0.270	**0.78**	2.9	8.4	62.3	18.0	42.5	12.4	74.9	156.8	5.2
	0.476	**11.34**	12.8	21.3	61.9	23.1	45.0	10.1	76.8	111.4	12.3
	0.750	**17.23**	16.3	23.9	52.8	21.1	46.4	9.1	74.8	89.4	14.2
	0.850	**25.66**	36.9	36.6	56.3	33.6	18.4	11.3	77.2	53.1	30.0
600	0.326	**8.13**	4.5	5.8	58.9	10.1	61.9	60.2	73.8	117.6	3.8
	0.528	**6.24**	4.3	22.2	59.8	20.3	51.0	43.2	76.8	70.8	9.7
	0.708	**8.54**	17.3	33.4	59.7	29.5	32.1	22.1	78.7	38.4	22.6
	0.850	**16.19**	26.5	35.9	55.3	31.4	22.5	11.8	77.4	27.1	27.7
Ave-MAE		**14.3**	16.5	26.3	26.3	27.8	32.1	27.4	77.1	103.1	13.1

$MAE = \frac{|HTC_{sim/corr} - HTC_{exp}|}{HTC_{exp}} \times 100$, $Ave - MAE = \frac{1}{N}\sum_{i=1}^{N} \frac{|HTC_{sim/corr,i} - HTC_{exp,i}|}{HTC_{exp,i}} \times 100$
(N: total number of cases = 12)

2.2. Deriving Heat Transfer Coefficient and Pressure Drop Correlations

Experimental investigations concerning the condensation flows of R600a and R290 inside microchannels are notably scarce in the existing literature. This scarcity is primarily attributed to the hazardous flammable and explosive characteristics associated with R600a and R290, which pose significant risks during experimental research. In the current study, new correlations for the heat transfer coefficient (HTC) and friction factor pertaining to R600a and R290 condensation flows inside microchannels are suggested. The new heat correlations are derived depending on the simulation data.

The new correlations were formulated based on the concept of the equivalent Reynolds number (Re_{eq}) [52], whose expressions can be found in Equations (15) and (16).

$$Re_{eq} = \frac{G_{eq} D_h}{\mu_l} \quad (15)$$

where the equivalent mass flux (G_{eq}) is defined as follows [52]:

$$G_{eq} = G\left[(1 - x) + x\sqrt{\frac{\rho_l}{\rho_v}}\right] \quad (16)$$

A power function curve fitting was employed to derive an equation capable of predicting the Nusselt number as a function of the equivalent Reynolds number. The new condensation heat transfer coefficient (HTC) correlations are suggested to be the condensation flows of R600a and R290 in the microchannel, in terms of the Nusselt number (Nu), as defined below.

$$\mathrm{Nu} = \frac{\mathrm{HTC\,D_h}}{\mathrm{k_l}} \tag{17}$$

Correlations for the pressure drop (Δp) are also derived in a similar manner, in terms of the friction factor (f), which is defined as in Equations (18) and (19).

$$\mathrm{f} = \Delta\mathrm{p}\frac{\mathrm{D_h}}{\mathrm{L}}\frac{2\rho_{\mathrm{TP}}}{\mathrm{G}^2} \tag{18}$$

where ρ_{TP} is the density of the two-phase mixture and is given as follows:

$$\rho_{\mathrm{TP}} = \frac{1}{(\mathrm{x}/\rho_{\mathrm{v}}) + ((1-\mathrm{x})/\rho_{\mathrm{l}})} \tag{19}$$

3. Results and Discussion

Experimental investigations concerning the condensation flow of hydrocarbon refrigerants (such as R600a and R290) inside microchannels are notably scarce in the existing literature. This scarcity is primarily attributed to the hazardous flammable and explosive characteristics associated with R600a and R290, which pose significant risks during experimental research. In other words, comprehensive and reliable data on the particular refrigerants R600a and R290 are notably lacking, despite their potential importance in the design of microchannel condensers. Consequently, the primary objective of this study is to offer a valuable contribution to the field by employing numerical simulations to define the heat transfer coefficient, as well as the pressure drop, for the condensation flow of R600a and R290 in microchannels. In the current study, new correlations for the heat transfer coefficient (HTC) and pressure drop pertaining to the R600a and R290 condensation flow inside microchannels are suggested.

A new heat transfer coefficient correlation is developed, which depends on the simulation data. Laminar and turbulent flow regimes can be obtained depending on the geometry and boundary conditions in microchannel applications. This necessitates consideration to obtain a better correlation accuracy. Although laminar and turbulent flows can occur independently for each phase, this study attempts to address this aspect in a simplified manner based on the equivalent Reynolds number (Equation (15)). It is assumed that the predominant flow behavior is laminar for Re $\leq$ 2300 and transitional or turbulent for Re > 2300. It is observed that nearly 19% (14 out of 72) of the investigated cases, particularly those with the 0.2 mm hydraulic diameter, formally fall into the laminar regime according to this definition. To develop the correlation, separate curve fits were performed using a power function for the two regimes. The following correlations were derived to predict the Nusselt number (Nu) as a function of the equivalent Reynolds number.

$$\mathrm{Nu} = \begin{cases} 0.2516 \times \mathrm{Re_{eq}^{0.6860}}, & \text{for } \mathrm{Re_{eq}} \leq 2300 \\ 0.3215 \times \mathrm{Re_{eq}^{0.6548}}, & \text{for } \mathrm{Re_{eq}} > 2300 \end{cases} \tag{20}$$

The new correlation was formulated based on the concept of the equivalent Reynolds number ($\mathrm{Re_{eq}}$), and its expressions can be found in Equations (15) and (16). A power function curve fitting was employed to derive an equation capable of predicting the Nusselt number as a function of the equivalent Reynolds number.

Figure 3 shows a comparison between Nusselt numbers computed using the newly formulated correlation (Equation (20)) and the Nusselt numbers computed by computational fluid dynamics (CFD) simulations. The dataset encompasses simulation results derived from diverse combinations of mass fluxes, inlet vapour quality, as well as hydraulic diameters, categorized based on the types of refrigerants. According to the comparison in Figure 3, the average mean absolute error (Ave-MAE) between the simulated and correlated

Nusselt number is within +/−30%. At low Nu numbers, a few points of R600a fall outside −30%. The Average Mean Absolute Error is computed as 11.16% for both R600a and R290.

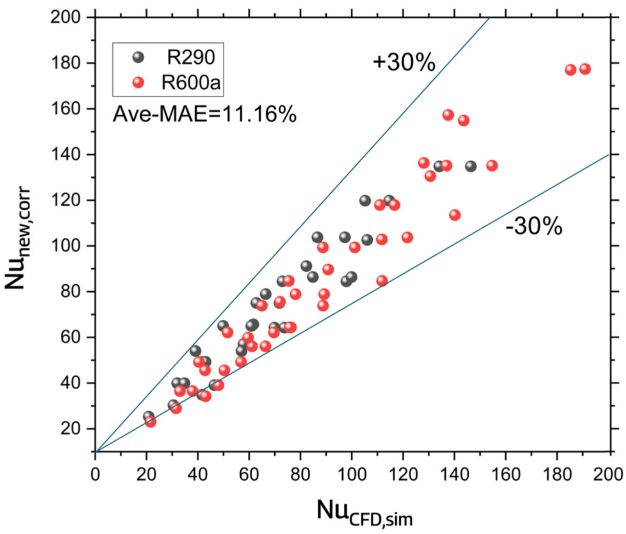

Figure 3. Comparison of Nu numbers provided by the newly developed correlation (Equation (20)) with those obtained by CFD simulation.

In order to evaluate the predictive accuracy of the recently formulated HTC correlation, a comparative analysis was carried out between the simulated Nusselt number and those computed from the pre-existing alternative Nusselt number correlations in the literature. Table 5 shows the deviations between the simulated Nusselt number and those computed from the pre-existing Nusselt number correlations in the literature. The pre-existing Nusselt number correlations, shown in Table 5, are widely recognized correlations of the heat transfer coefficient for refrigerant condensation within small-scale channels. Their details and application range are provided in Table 1. According to Table 5, the newly proposed HTC correlation has a better prediction performance than the other correlations. Its deviation has an 11.16% Ave-MAE. Table 5 shows that the new HTC correlation has the best prediction performance for all investigated diameter and refrigerants compared to the other considered correlations. The deviations of the new correlation in the condensation flows of both R290 and R600a at 0.2 mm diameter are higher than the deviations at 0.4 and 0.6 mm diameters. However, these deviations (18.21% for R290/D = 0.2 mm; 13.61% for R600a/D = 0.2 mm) are still lower than the deviations of other correlations at a 0.2 mm diameter for refrigerants. The newly developed correlation shows lower deviations for the condensation flow of R600a with 0.2 and 0.4 mm diameters compared to the condensation flow of R290 with the same diameter.

A comparison between the Nu numbers predicted by the new correlation and those calculated using pre-existing alternative Nusselt number correlations in the literature was also conducted. The comparison is provided in Figure 4 and the comparison shows the predictions of both R600a and R290. In Figure 4, $Nu_{new,corr}$ represents the Nu numbers predicted by the new correlation while Nu_{corr} denotes the Nu numbers calculated using pre-existing alternative Nusselt number correlations. According to Figure 4, the newly proposed heat transfer coefficient correlation for microchannel condensation flow shows similar predictions to those of Son and Lee [16], with 17.39% Ave-MAE, and Dobson and Chato [12], with 19.14% Ave-MAE. This is followed by those of Shah [20], with 28.38% Ave-MAE, Cavallini et. al. [15], with 35.61% Ave-MAE, and Moser et. Al., with 37.24% Ave-MAE, respectively. Other correlations have an Ave-MAE that is higher than 50% compared to the Nu number predictions of the new correlation.

Table 5. The deviations between the simulated Nusselt number and those computed from the pre-existing Nusselt number correlations in the literature.

Refrigerant/ Diameter	MAE of Condensation HTC Correlations (%)									
	New HTC Correlation	Dobson and Chato [12]	Moser et al. [13]	Koyama et al. [14]	Cavallini et al. [15]	Son and Lee [16]	Huang et al. [17]	Park et al. 2011 [18]	Bohdal et al., 2011 [19]	Shah, 2016 [20]
R290/D = 0.2 mm	18.21	23.50	38.34	66.69	41.91	19.08	87.67	84.85	135.43	33.05
R290/D = 0.4 mm	9.51	18.15	35.92	64.58	37.94	18.90	55.55	83.66	74.15	28.69
R290/D = 0.6 mm	8.92	21.15	38.71	65.77	39.96	20.89	39.32	83.98	35.60	31.18
R600a/D = 0.2 mm	13.61	19.01	36.74	60.88	32.62	20.04	181.19	76.07	114.48	26.51
R600a/D = 0.4 mm	6.57	15.27	34.86	59.20	29.24	29.24	125.73	75.26	54.09	23.14
R600a/D = 0.6 mm	10.17	17.14	36.11	59.98	30.21	19.97	93.25	75.72	23.02	24.35
Ave-MAE	**11.16**	**19.04**	**36.78**	**62.85**	**35.31**	**21.35**	**97.12**	**79.92**	**72.80**	**27.82**

$$\mathrm{MAE} = \frac{|\mathrm{HTC_{corr}} - \mathrm{HTC_{sim}}|}{\mathrm{HTC_{sim}}} \times 100, \quad \mathrm{Ave-MAE} = \frac{1}{N}\sum_{i=1}^{N} \frac{|\mathrm{HTC_{corr,i}} - \mathrm{HTC_{sim,i}}|}{\mathrm{HTC_{sim,i}}} \times 100$$

(N: total number of cases = 72)

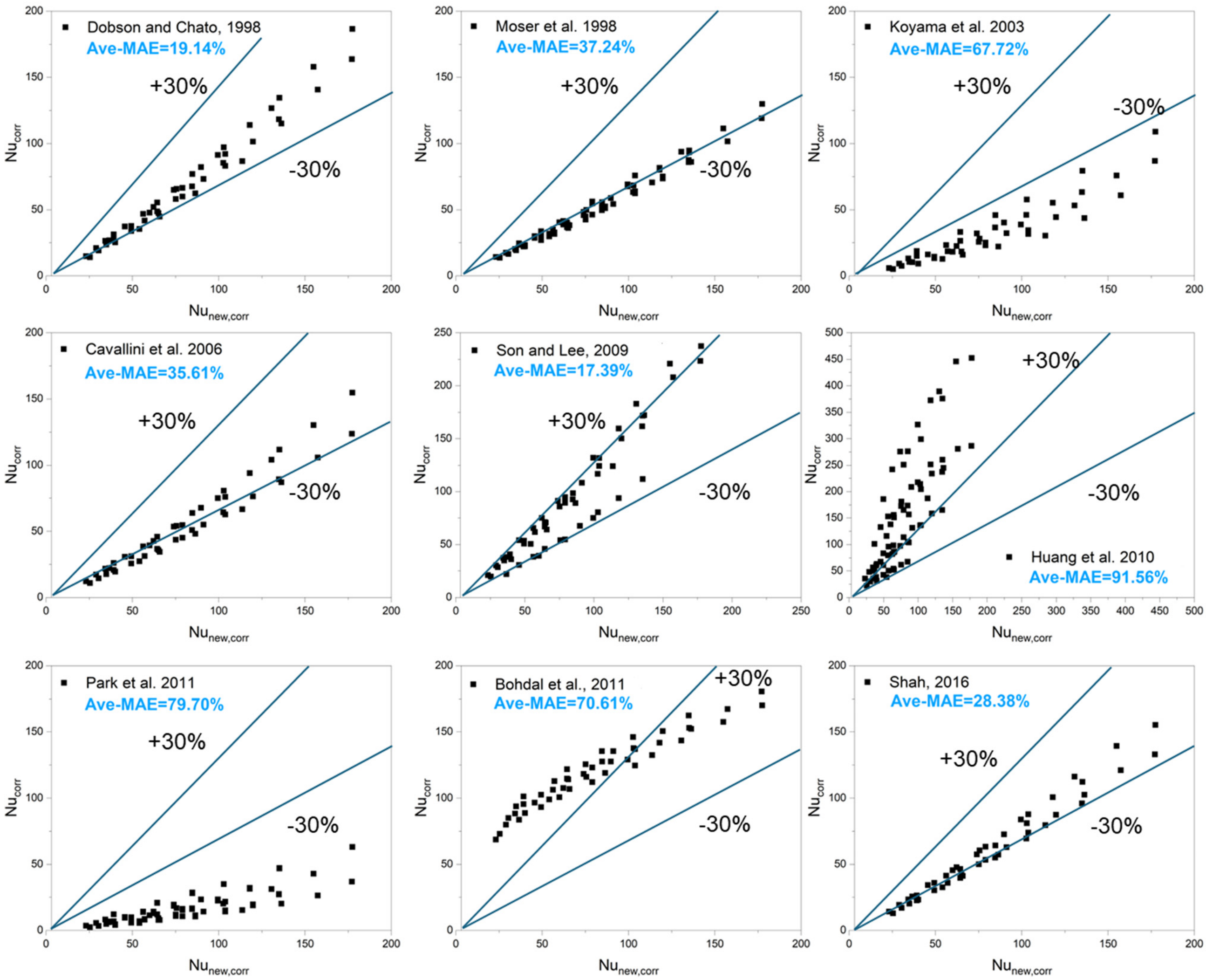

Figure 4. Comparison of the Nu numbers provided by the newly developed correlation (Equation (20)) with those obtained by pre-existing Nusselt number correlations in the literature [12–20].

A new pressure drop correlation was also derived depending on the simulation data. The correlation was developed in terms of the friction factor (Equation (18)). The correlations derived for the friction factor in both the laminar and transitional/turbulent regimes are presented below:

$$f = \begin{cases} 0.8393 \times Re_{eq}^{-0.2200}, & Re_{eq} \leq 2300 \\ 0.7344 \times Re_{eq}^{-0.2260}, & Re_{eq} > 2300 \end{cases} \tag{21}$$

Figure 5 indicates a comparison between pressure drops computed via the new correlation (Equation (21)) and the simulated ones. It can be seen in Figure 5 that the MAE between newly derived correlation and CFD simulations is within +/−30%, except for three data points of R600a and one data point of R290. Ave-MAE, which covers all data points of both refrigerants, is 20.81%.

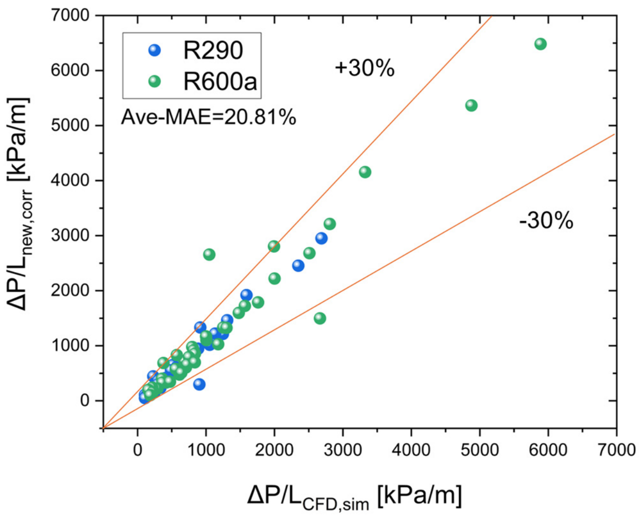

Figure 5. Comparison of pressure drop provided by the newly developed correlation (Equation (21)) with those obtained by CFD simulation.

To evaluate the prediction ability of the proposed correlation, a comparison is made between the friction factor obtained by CFD simulation data and the friction factors obtained by the already existing correlations. The existing correlations, shown in Table 6, are alternative pressure drop correlations that can be applied to the condensation flow inside the refrigerants. The application range of these correlations is shown in Table 2. Table 6 shows that the new correlation has the best overall prediction performance of all existing correlations, with a 20.81% Ave-MAE. For all investigated cases, the deviations of newly the derived correlations are the same as the deviations of other correlations. For both R290 and R600a refrigerants, the predictions of the new correlations show higher deviations at a flow of 0.2 mm than the deviations of condensation flows of 0.4 and 0.6 mm. However, the deviations of new correlations for a 0.2 mm diameter remain lower than the deviations of other correlations.

The pressure drops predicted by new correlations and those computed using pre-existing alternative Nusselt number correlations in the literature were also compared. The comparison covers data points of both R600a and R290 and is shown in Figure 6. In Figure 6, $\Delta P/L_{new,corr}$ denotes the pressure drop predicted by the new correlation, whereas $\Delta P/L_{corr}$ stands for the pressure drop computed using pre-existing alternative pressure drop correlations. Figure 6 shows that, for microchannel condensation flow, Lockhart and Martinelli [21] show similar predictions to those obtained by the new pressure drop, with 37.16% Ave-MAE. This is followed by those of Cavallini et al. [25], with 38.87% Ave-MAE. Other correlations indicate an Ave-MAE of higher than 50% compared to the pressure drop predictions of the new correlation.

Table 6. The deviations between the simulated friction factor and those computed from the pre-existing friction factor correlations in the literature.

Refrigerant/ Diameter	MAE of Condensation Friction Factor Correlations (%)									
	New HTC Correlation	Lockhart and Martinelli [21]	Friedel [22]	Mishima and Hibiki [23]	Cavallini et al. [25]	Garimella et al. [24]	Bohdal et al. [19]	Son and Oh [26]	Sakamatapan and Wongmisses [27]	Lopez-Belchi et al. [28]
R290/D = 0.2 mm	25.81	28.99	47.40	72.56	41.88	50.88	190.34	79.27	133.32	74.59
R290/D = 0.4 mm	10.19	34.70	58.23	72.91	49.53	46.47	49.85	40.37	87.39	77.36
R290/D = 0.6 mm	22.98	46.36	63.61	74.07	57.54	52.32	13.09	51.42	62.20	79.56
R600a/D = 0.2 mm	38.29	32.99	33.51	72.57	63.26	49.98	209.83	78.11	29.31	68.33
R600a/D = 0.4 mm	9.88	40.47	54.15	73.83	30.14	52.43	59.49	45.33	18.69	71.51
R600a/D = 0.6 mm	17.70	52.97	62.37	74.64	42.78	53.82	38.66	56.58	30.43	73.69
Ave-MAE	**20.81**	**39.41**	**53.21**	**73.43**	**47.52**	**50.99**	**93.54**	**58.51**	**60.22**	**74.17**

$$\mathrm{MAE} = \frac{|f_{corr} - f_{sim}|}{f_{sim}} \times 100, \quad \mathrm{Ave-MAE} = \frac{1}{N}\sum_{i=1}^{N} \frac{|f_{corr,i} - f_{sim,i}|}{f_{sim,i}} \times 100$$

(N: total number of cases = 72)

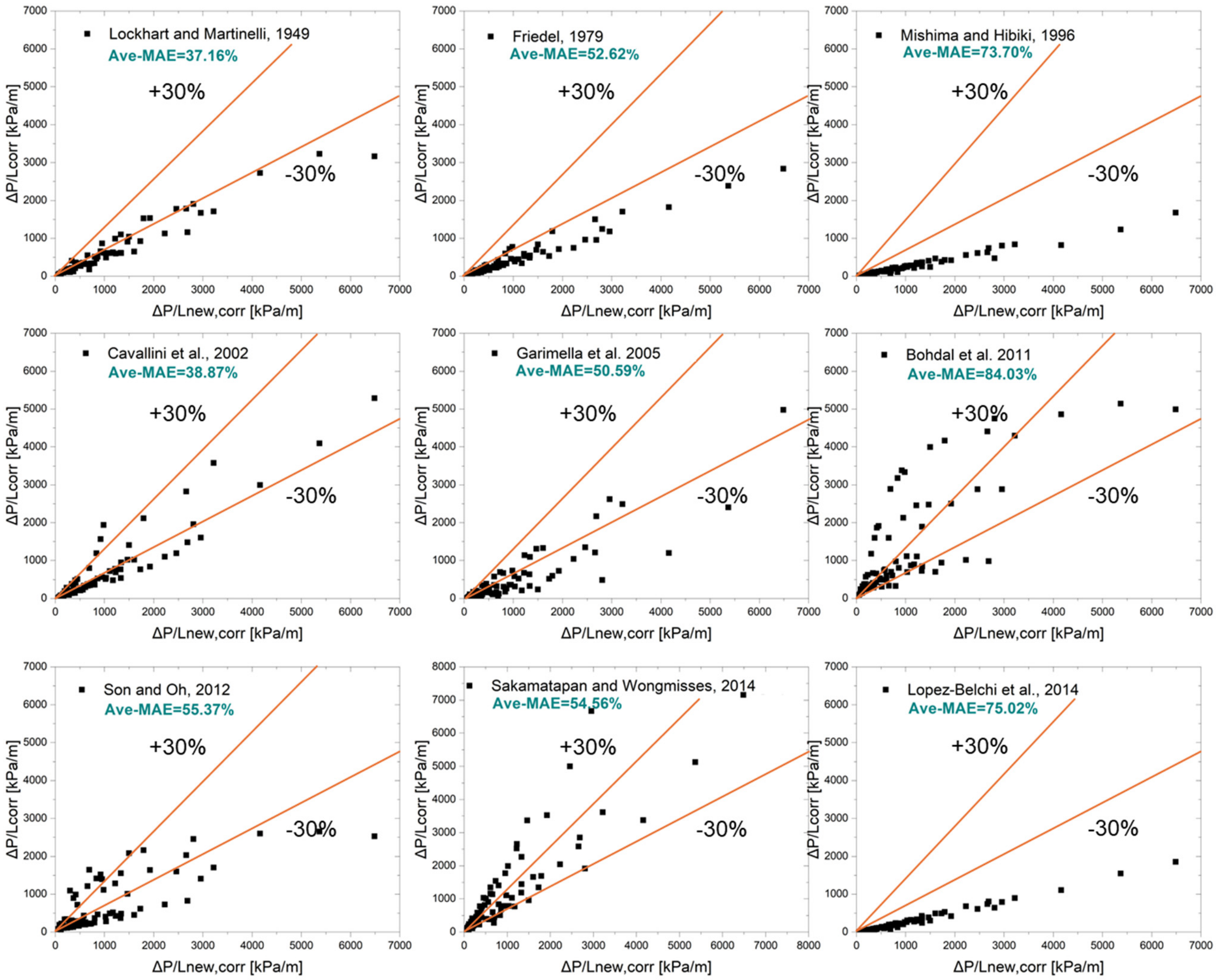

Figure 6. Comparison of the pressure drop provided by the newly developed correlation (Equation (21)) with those obtained by pre-existing pressure drop correlations in the literature [19,21–28].

The data points employed in the development of new correlations cover the simulation results based on various mass fluxes and hydraulic diameters, classified in terms of the hydraulic diameters of refrigerants R290 and R600a. In this respect, the application ranges of the newly proposed correlations are summarized in Table 7.

Table 7. Application ranges of the new correlations.

Formula	Application Range
Nusselt number for heat transfer coefficient: $Nu = \begin{cases} 0.2516 \times Re_{eq}^{0.6860}, & \text{for } Re_{eq} \leq 2300 \\ 0.3215 \times Re_{eq}^{0.6548}, & \text{for } Re_{eq} > 2300 \end{cases}$ Friction factor for pressure drop: $f = \begin{cases} 0.8393 \times Re_{eq}^{-0.2200}, & Re_{eq} \leq 2300 \\ 0.7344 \times Re_{eq}^{-0.2260}, & Re_{eq} > 2300 \end{cases}$	R290 and R600a G = 200–600 kg/m^2s T_{sat} = 40 °C x = 0.3–0.9 D_h = 0.2–0.6 mm

4. Conclusions

In this study, a numerical analysis was carried out of the condensation flows of R600a and R290 through a circular microchannel. The main motivation was the knowledge gap regarding the condensation of these refrigerants in microchannels. The proposed numerical model was verified using the available experimental data on R134a condensation in the microchannel under steady-state film condensation. New correlations for heat transfer coefficient and pressure drop were developed for R600a and R290 condensation inside microchannels based on the simulation results. This endeavor effectively addressed a notable void in the existing literature and fulfilled the demand for accurate predictive models, which are essential for the design of heat exchangers. Consequently, this research aids in the development of high-efficiency condensers that employ environmentally friendly refrigerants that are extensively employed in HVAC-R systems. The key conclusions are summarized below:

- Based on the results of the CFD simulations, new correlations are suggested for the heat transfer coefficient (expressed as Nu) and the pressure drop (expressed as f) in the context of R600a and R290 condensation within microchannels. It is concluded that the newly developed heat transfer and pressure drop correlations demonstrate the best agreement with the simulations when compared to alternative correlations from the literature.
- In terms of heat transfer coefficient, the proposed new correlation achieves the lowest deviation, with an Ave-MAE of 11.16%, followed by the correlation of Dobson and Chato [12] (MAE = 19.04%). Similarly, the new pressure drop correlation exhibits the closest overall agreement with the simulation results compared to alternative correlations available in the literature, with an Ave-MAE of 20.81%. This is followed by the correlation of Lockhart and Martinelli [21], with 39.41% Ave-MAE.
- It is found that, in parallel with the comparison of the CFD simulation results, Dobson and Chato [12] and Lockhart and Martinelli [21] made predictions that are the closest to the new correlations in terms of heat transfer coefficient and pressure drop, respectively.
- It can be concluded that, in contrast to existing correlations, the proposed correlations have a higher potential for accurately predicting pressure drop and heat transfer coefficients for R600a and R290 condensation within microchannels. These new correlations, which are easily applicable, may contribute to the design of microchannel condensers operating with R600a and/or R290. They can be used to design tools to enhance refrigeration, heat pumps, HVAC, electronic cooling devices, etc.

Author Contributions: Conceptualization, A.B. and A.C.B.; methodology, A.B. and A.C.B.; validation, A.B.; investigation, A.B.; writing—original draft preparation, A.B.; writing—review and editing, A.C.B.; supervision, A.C.B. All authors have read and agreed to the published version of the manuscript.

Funding: This research received no external funding.

Data Availability Statement: The raw data supporting the conclusions of this article will be made available by the authors on request.

Conflicts of Interest: The authors declare no conflicts of interest. The funders had no role in the design of the study; in the collection, analyses, or interpretation of data; in the writing of the manuscript; or in the decision to publish the results.

Nomenclature

Bo	Bond number = $g(\rho_l - \rho_v)D_h^2/\sigma$
Bo_{cr}	Critical Bond number = $[\rho_l/(\rho_1 - \rho_v) - \pi/4]$
C	Chisholm factor
D	Diameter, m
D_h	Hydraulic diameter, m
D_v	Vapor core diameter, m
EU	European Union
f	Friction factor
Fr	Froude number = $G^2/gD_h\rho^2$
Fr_{so}	Soliman Froude number
Fr_{TP}	Two-phase mixture Froude number = $G^2/gD_h\rho_{TP}^2$
$\vec{F}_{vol}$	Volume force due to surface tension, N m^{-3}
g	Gravity acceleration, kg-s^{-2}
G	Mass flux, kg m^{-2} s^{-1}
GWP	Global warming potential
h	Enthalpy, J kg^{-1}
h_{lv}	Latent heat, J kg^{-1}
HC	HydroCarbon
HFC	HydroFluoroCarbon
HTC	Heat transfer coefficient, W m^{-2} K^{-1}
k_l	Thermal conductivity of the liquid phase, W m^{-1} K^{-1}
L	Tube length, m
MCHE	Microchannel heat exchanger
Nu	Nusselt number = hD_h/k_l
p	Pressure, Pa
Pr	Prandtl number
Re_{eq}	All liquid Reynolds numbers = $G_{eq}D_h/\mu_l$
Re_l	Liquid Reynolds number = $GD_h(1-x)/\mu_l$
Re_{lo}	All liquid Reynolds numbers = GD_h/μ_l
Re_{TP}	Two-phase mixture Reynolds number = GD_h/μ_{TP}
Re_v	Vapour Reynolds number = GD_hx/μ_v
Re_{vo}	All vapour Reynolds numbers = GD_h/μ_v
S	Mass source term, kg m^{-3} s^{-1}
S_E	Energy source term, J m^{-3} s^{-1}
T	Temperature, °C
u	Velocity, m s^{-1}
VOF	Volume of fluid
We	Weber number = $G^2D_h/\rho\sigma$
We_{TP}	Two-phase mixture Weber number = $G^2D_h/\rho_{TP}^2\sigma$
x	Vapour quality
X_{tt}	Lockhart–Martinelli parameter = $(\rho_v/\rho_l)^{0.5}(\mu_l/\mu_v)^{0.1}((1-x)/x)^{0.9}$
Greek symbols	
α	Volume fraction
$\propto$	Void fraction
β	Tunable positive numerical coefficient, s^{-1}
κ_L	Interface curvature
μ	Dynamic viscosity, Pa s
μ_{TP}	Two-phase mixture viscosity = $[(1/\mu_v) + (1-x)/\mu_l)]^{-1}$
ρ	Density, kg m^{-3}

ρ_{TP}	Two-phase mixture density = $[(1/\rho_v) + (1-x)/\rho_l)]^{-1}$
σ	Surface tension, N m^{-1}
φ	Fluid properties
λ	Thermal conductivity, W m^{-1} K^{-1}
∅	Two-phase multiplier
Subscripts	
cr	Critical
eff	Effective
eq	Equivalent
l	Liquid
lo	All-liquid
sat	Saturation
v	Vapour
vo	All-vapour

References

1. Xue, M.; Kojima, N.; Zhou, L.; Machimura, T.; Tokai, A. Trade-off Analysis between Global Impact Potential and Local Risk: A Case Study of Refrigerants. *J. Clean. Prod.* **2019**, *217*, 627–632. [CrossRef]
2. Xue, M.; Kojima, N.; Machimura, T.; Tokai, A. Flow, Stock, and Impact Assessment of Refrigerants in the Japanese Household Air Conditioner Sector. *Sci. Total Environ.* **2017**, *586*, 1308–1315. [CrossRef] [PubMed]
3. EU F-Gas Regulation 517/2014. Regulation (EU) No 517/2014 of the European Parliament and of the Council of 16 April 2014 on Fluorinated Greenhouse Gases and Repealing Regulation (EC) No 842/2006. *Off. J. Eur. Union* **2014**, *2014*, L150/195-230.
4. Basaran, A.; Benim, A.C.; Yurddas, A. Numerical Simulation of the Condensation Flow of the Isobutane (R600a) inside Microchannel. *Heat Transf. Eng.* **2021**, *43*, 337–361. [CrossRef]
5. Başaran, A.; Yurddaş, A. Thermal Modeling and Designing of Microchannel Condenser for Refrigeration Applications Operating with Isobutane (R600a). *Appl. Therm. Eng.* **2021**, *198*, 117446. [CrossRef]
6. Başaran, A. Experimental Investigation of R600a as a Low GWP Substitute to R134a in the Closed-Loop Two-Phase Thermosyphon of the Mini Thermoelectric Refrigerator. *Appl. Therm. Eng.* **2022**, *211*, 118501. [CrossRef]
7. Kandlikar, S.G. A Roadmap for Implementing Minichannels in Refrigeration and Air-Conditioning Systems—Current Status and Future Directions. *Heat Transf. Eng.* **2007**, *28*, 973–985. [CrossRef]
8. Roth, K.; Westphalen, D.; Dieckmann, J.; Hamilton, S.; Goetzler, W. *Energy Consumption Characteristics of Commercial Building HVAC Systems, Volume III: Energy Savings Potential*; Tıax, LLC.: Cambridge, MA, USA, 2002; Volume 3.
9. Ghiassiaan, S.M. *Two-Phase Flow, Boiling, and Condensation in Conventional and Minature Systems*; Cambridge University Press: Cambridge, UK, 2008; ISBN 9780511619410.
10. Kandlikar, S.G.; Colin, S.; Peles, Y.; Garimella, S.; Pease, R.F.; Brandner, J.J.; Tuckerman, D.B. Heat Transfer in Microchannels—2012 Status and Research Needs. *J. Heat Transf.* **2013**, *135*, 091001. [CrossRef]
11. Basaran, A.; Benim, A.C.; Yurddas, A. Prediction of Heat and Fluid Flow in Microchannel Condensation. *E3S Web Conf.* **2019**, *128*, 01015. [CrossRef]
12. Dobson, M.K.; Chato, J.C. Condensation in Smooth Horizontal Tubes. *J. Heat Transf.* **1998**, *120*, 193–213. [CrossRef]
13. Moser, K.W.; Webb, R.L.; Na, B. A New Equivalent Reynolds Number Model for Condensation in Smooth Tubes. *J. Heat Transf.* **1998**, *120*, 410–417. [CrossRef]
14. Koyama, S.; Kuwahara, K.; Nakashita, K.; Yamamoto, K. An Experimental Study on Condensation of Refrigerant R134a in Multi-Port Extruded Tube. *Int. J. Refrig.* **2003**, *26*, 425–432. [CrossRef]
15. Cavallini, A.; Doretti, L.; Matkovic, M.; Rossetto, L. Update on Condensation Heat Transfer and Pressure Drop inside Minichannels. *Heat Transf. Eng.* **2006**, *27*, 74–87. [CrossRef]
16. Son, C.-H.; Lee, H.-S. Condensation Heat Transfer Characteristics of R-22, R-134a and R-410A in Small Diameter Tubes. *Heat Mass Transf.* **2009**, *45*, 1153–1166. [CrossRef]
17. Huang, X.; Ding, G.; Hu, H.; Zhu, Y.; Peng, H.; Gao, Y.; Deng, B. Influence of Oil on Flow Condensation Heat Transfer of R410A inside 4.18 Mm and 1.6 Mm Inner Diameter Horizontal Smooth Tubes. *Int. J. Refrig.* **2010**, *33*, 158–169. [CrossRef]
18. Park, J.E.; Vakili-Farahani, F.; Consolini, L.; Thome, J.R. Experimental Study on Condensation Heat Transfer in Vertical Minichannels for New Refrigerant R1234ze(E) versus R134a and R236fa. *Exp. Therm. Fluid. Sci.* **2011**, *35*, 442–454. [CrossRef]
19. Bohdal, T.; Charun, H.; Sikora, M. Comparative Investigations of the Condensation of R134a and R404A Refrigerants in Pipe Minichannels. *Int. J. Heat Mass. Transf.* **2011**, *54*, 1963–1974. [CrossRef]
20. Shah, M.M. Comprehensive Correlations for Heat Transfer during Condensation in Conventional and Mini/Micro Channels in All Orientations. *Int. J. Refrig.* **2016**, *67*, 22–41. [CrossRef]
21. Lockhart, R.; Martinelli, R. Proposed Correlation of Data for Isothermal Two-Phase, Two-Component Flow in Pipes. *Chem. Eng. Prog.* **1949**, *45*, 29–48.
22. Friedel, L. Improved Friction Pressure Drop Correlation for Horizontal and Vertical Two-Phase Pipe Flow. In Proceedings of the European Two-Phase Group Meeting, Ispra, Italy, 5–8 June 1979.

23. Mishima, K.; Hibiki, T. Some Characteristics of Air-Water Two-Phase Flow in Small Diameter Vertical Tubes. *Int. J. Multiph. Flow* **1996**, *22*, 703–712. [CrossRef]
24. Garimella, S.; Agarwal, A.; Killion, J.D. Condensation Pressure Drop in Circular Microchannels. *Heat Transf. Eng.* **2005**, *26*, 28–35. [CrossRef]
25. Cavallini, A.; Censi, G.; Del Col, D.; Doretti, L.; Longo, G.A.; Rossetto, L. Condensation of Halogenated Refrigerants inside Smooth Tubes. *HVAC R Res.* **2002**, *8*, 429–451. [CrossRef]
26. Son, C.; Oh, H. Condensation Pressure Drop of R22, R134a and R410A in a Single Circular Microtube. *Heat Mass Transf.* **2012**, *48*, 1437–1450. [CrossRef]
27. Sakamatapan, K.; Wongwises, S. Pressure Drop during Condensation of R134a Flowing inside a Multiport Minichannel. *Int. J. Heat Mass Transf.* **2014**, *75*, 31–39. [CrossRef]
28. López-belchí, A.; Illán-gómez, F.; Vera-garcía, F.; García-cascales, J.R. Experimental Condensing Two-Phase Frictional Pressure Drop inside Mini-Channels. Comparisons and New Model Development. *Int. J. Heat Mass Transf.* **2014**, *75*, 581–591. [CrossRef]
29. Li, L.; Li, Q.; Ni, Y.; Wang, C.; Tan, Y.; Tan, D. Critical Penetrating Vibration Evolution Behaviors of the Gas-Liquid Coupled Vortex Flow. *Energy* **2024**, *292*, 130236. [CrossRef]
30. Li, L.; Xu, W.; Tan, Y.; Yang, Y.; Yang, J.; Tan, D. Fluid-Induced Vibration Evolution Mechanism of Multiphase Free Sink Vortex and the Multi-Source Vibration Sensing Method. *Mech. Syst. Signal Process* **2023**, *189*, 110058. [CrossRef]
31. Chen, S.; Yang, Z.; Duan, Y.; Chen, Y.; Wu, D. Simulation of Condensation Flow in a Rectangular Microchannel. *Chem. Eng. Process. Process Intensif.* **2014**, *76*, 60–69. [CrossRef]
32. Ganapathy, H.; Shooshtari, A.; Choo, K.; Dessiatoun, S.; Alshehhi, M.; Ohadi, M. Volume of Fluid-Based Numerical Modeling of Condensation Heat Transfer and Fluid Flow Characteristics in Microchannels. *Int. J. Heat Mass Transf.* **2013**, *65*, 62–72. [CrossRef]
33. Bortolin, S.; Da Riva, E.; Del Col, D. Condensation in a Square Minichannel: Application of the VOF Method. *Heat Transf. Eng.* **2014**, *35*, 193–203. [CrossRef]
34. Zhang, J.; Li, W.; Minkowycz, W.J. Numerical Simulation of Condensation for R410A at Varying Saturation Temperatures in Mini/Micro Tubes. *Numer. Heat. Transf. A Appl.* **2016**, *69*, 464–478. [CrossRef]
35. Toninelli, P.; Bortolin, S.; Azzolin, M.; Del Col, D. Visualization and Numerical Simulations of Condensing Flow in Small Diameter Channels. *Heat Transf. Eng.* **2019**, *40*, 802–817. [CrossRef]
36. Wu, C.; Li, J. Numerical Simulation of Flow Patterns and the Effect on Heat Flux during R32 Condensation in Microtube. *Int. J. Heat Mass Transf.* **2018**, *121*, 265–274. [CrossRef]
37. Da Riva, E.; Del Col, D. Effect of Gravity during Condensation of R134a in a Circular Minichannel: VOF Simulation of Annular Condensation. *Microgravity Sci. Technol.* **2011**, *23*, 87–97. [CrossRef]
38. Da Riva, E.; Del Col, D. Numerical Simulation of Laminar Liquid Film Condensation in a Horizontal Circular Minichannel. *J. Heat Transf.* **2012**, *134*, 051019. [CrossRef]
39. ASHRAE. *American Society of Heating Refrigerating and Air Conditioning Engineers (ASHRAE) Handbook-Fundamentals*; ASHRAE Inc.: Atlanta, GA, USA, 2009.
40. Coleman, J.W.; Garimella, S. Two-Phase Flow Regimes in Round, Square and Rectangular Tubes during Condensation of Refrigerant R 134a. *Int. J. Refrig.* **2003**, *26*, 117–128. [CrossRef]
41. Li, J.M.; Wang, B.X. Size Effect on Two-Phase Regime for Condensation in Micro/Mini Tubes. *Heat Transf. Asian Res.* **2003**, *32*, 65–71. [CrossRef]
42. Nema, G.; Garimella, S.; Fronk, B.M. Flow Regime Transitions during Condensation in Microchannels. *Int. J. Refrig.* **2014**, *40*, 227–240. [CrossRef]
43. Hirt, C.W.; Nichols, B.D. Volume of Fluid (VOF) Method for the Dynamics of Free Boundaries. *J. Comput. Phys.* **1981**, *39*, 201–225. [CrossRef]
44. Brackbill, J.U.; Kothe, D.B.; Zemach, C. A Continuum Method for Modeling Surface Tension. *J. Comput. Phys.* **1992**, *100*, 335–354. [CrossRef]
45. *ANSYS® FLUENT, Release 2023-R1*; Academic Version; Ansys: Canonsburg, PA, USA, 2023.
46. Durbin, P.A.; Reif, B.A.P. *Statistical Theory and Modeling for Turbulent Flows*; John Wiley & Sons: Hoboken, NJ, USA, 2011; ISBN 1119957524.
47. Benim, A.C. Finite Element Analysis of Confined Turbulent Swirling Flows. *Int. J. Numer. Method. Fluids* **1990**, *11*, 697–717. [CrossRef]
48. Xia, J.L.; Smith, B.L.; Benim, A.C.; Schmidli, J.; Yadigaroglu, G. Effect of Inlet and Outlet Boundary Conditions on Swirling Flows. *Comput. Fluids* **1997**, *26*, 811–823. [CrossRef]
49. Bhattacharyya, S.; Benim, A.C.; Pathak, M.; Chamoli, S.; Gupta, A. Thermohydraulic Characteristics of Inline and Staggered Angular Cut Baffle Inserts in the Turbulent Flow Regime. *J. Therm. Anal. Calorim.* **2020**, *140*, 1519–1536. [CrossRef]
50. Menter, F.R. Two-Equation Eddy-Viscosity Turbulence Models for Engineering Applications. *AIAA J.* **1994**, *32*, 1598–1605. [CrossRef]

51. Shin, J.S.; Kim, M.H. An Experimental Study of Flow Condensation Heat Transfer Inside Circular and Rectangular Mini-Channels. *Heat Transf. Eng.* **2005**, *26*, 633–640. [CrossRef]
52. Akers, W.W.; Deans, H.A.; Crosser, O.K. Condensation Heat Transfer within Horizontal Tubes. *Chem. Eng. Prog. Symp. Ser.* **1959**, *55*, 171–176.